TECHNICAL ARTICLE

Tribological Evaluation of NbC and VC Layers Produced by Thermo-Reactive Diffusion Treatment in Ductile Cast Irons with Varying Composition

Fábio Edson Mariani, Amadeu Neto Lombardi, and Luiz Carlos Casteletti

Influence of Cu-Ni-Mo alloying on the wear characteristics of ADI (Austempered Ductile Iron) was studied. Additionally, its influence on the formation of NbC and VC layers (produced by means of thermo-reactive diffusion treatment TRD) on the ADI samples, and layer wear characteristics were investigated. Four ductile cast irons samples were used, the reference sample with no alloying and three others alloyed with Cu, Cu-Ni and Cu-Ni-Mo, respectively. For layer production, molten salt baths composed of sodium borate, aluminum and ferro-alloy (Fe-Nb or Fe-V), at 1000 °C during a 2-h treatment were used. Since the high TRD temperature was responsible for the austenitization of the sample, an austempering treatment direct from the TRD bath was performed immediately afterward using another molten salt bath at 300 °C. Sample examination and analysis were performed by optical and SEM microscopy, EDX, XRD, Brinell and Vickers hardness, Daimler-Benz Rockwell-C adhesion testing and fixed ball type micro-adhesive wear tests. TRD treatments were highly efficient in the production of robust uniform carbide layers with good adhesion to the substrates in all the samples. Wear resistance of the carbide layers was much greater than the austempered only substrates indicating the effectiveness of the TRD treatment for the materials studied.

1. Introduction

Mechanical component wear is one of the main problems encountered in industrial manufacturing processes. This fact has led to substantial scientific and technical effort in the development of surface layers or coatings with superior performance. These surface treatments offer the most versatile alternative to improve surface wear performance with good component surface properties combined with mechanical properties of the substrate (Ref 1-3).

Among the materials used in industry to manufacture mechanical parts and components, ductile cast irons are used for their low cost and possibility of being subjected to heat treatments to significantly increase their properties. Among the treatments available, austempering enables the production of Austempered Ductile Iron (ADI) which has an outstanding combination of mechanical properties. The hardness, strength and toughness in addition to good strength/weight ratio make

ADI a potential substitute for forged steel components in various mechanical applications (Ref 2-4).

ADIs are produced by austenitization of ductile cast iron above 850 °C followed by cooling in a salt bath between 230 and 400 °C. Due to the high concentration of carbon and silicon, transformation of austenite during the austempering process behaves differently relative to the same treatment performed on carbon steels (Ref 3, 5, 6).

During austempering of ductile cast iron, ferrite plates nucleate and grow in the contours of primary austenite grains being separated by thin layers of carbon saturated austenite. Over time, carbon saturation in austenite increases and its diffusion becomes more difficult, causing plate growth to cease. The remaining high carbon austenite becomes stable and the material can be cooled to room temperature without the formation of martensite or cementite. The result of the treatment is a microstructure consisting of retained austenite and acicular ferrite called ausferrite (Ref 3-6).

Recent studies observed that the performance of ADIs can be optimized with the production of high performance surface layers with characteristics far superior to those of the substrate (Ref 1-3). Among the processes used for layers production, thermoreactive diffusion treatment (TRD) stands out because it allows austempering to be performed directly from the treatment temperature. The objective of this treatment technique is the direct production of a layer with excellent properties over an austempered substrate without the need for further reheating which can result in significant savings in cost and production time (Ref 1).

TRD in a liquid medium uses sodium borate (borax) as the main component for the production bath, with the addition of ferro-alloys, to obtain carbide layers (Ref 3, 7, 8). TRD treatments are used to produce layers of NbC, VC and Cr-C on

Fábio Edson Mariani and **Luiz Carlos Casteletti**, Materials Engineering Department, University of São Paulo / São Carlos School of Engineering, Sao Carlos, Sao Paulo, Brazil; and **Amadeu Neto Lombardi**, Materials Engineering Department, Federal University of Technology - Paraná, Londrina, Parana, Brazil. Contact e-mail: mariani.fabioe@gmail.com.

ferrous substrates that contain > 0.3 wt.% carbon. In this process, elements such as niobium, vanadium, chromium or a mixture is added in the salt bath and combined chemically with the carbon of the substrate producing carbide layers (Ref 7-12).

The objective of this work consisted of the production and tribological evaluation of NbC and VC layers obtained by means of TRD treatment in four cast irons samples to verify the influence of their chemical compositions and the effectiveness of performing direct austempering from the thermoreactive treatment temperature.

2. Materials and Methods

In this work, four pearlitic ductile cast irons (chemical compositions are presented in Table 1) were used: one unalloyed and the other three alloyed with Cu, Cu-Ni and Cu-Ni-Mo, respectively, with dimensions of $30 \times 20 \times 5$ mm. The samples prior to the treatment were sanded with SiC sandpaper up to 400 mesh and cleaned in an ultrasonic bath with ethyl alcohol.

The TRD salt baths used to produce the layers were composed of aluminum (3 wt.%), Fe-Nb or Fe-V (16 wt.%) and borax-$Na_2B_4O_7$ (81 wt%). The chemical compositions of the metallic components of the salt bath are presented in Table 2.

Fe-Nb or Fe-V with particle sizes less than 45 μm were added to the baths in powder form. The temperature used for the TRD treatments was 1000 °C with a 2 h residence time in an AISI 316 stainless steel crucible (chemical composition in wt.%: 0.08 C, 0.70 Si, 2.00 Mn, 2.50 Mo, 12.00 Ni, 17.00 Cr). Austempering treatments were performed in an austempering salt bath at a temperature of 300 °C with a 4 h residence time.

2.1 Metallographic Preparation

The metallographic preparation followed the conventional procedures of cutting, embedding, sanding, polishing and chemical attack. The cut was made transversely to the treated surface of the samples, using a cut-off with a diamond abrasive disk at 300 RPM, followed by hot inlay with bakelite edge retention, sanding in SiC sandpaper up to 1500 mesh and polishing with aqueous solutions of 1.00, 0.25 and 0.05 μm alumina. After polishing, the samples were cleaned in a bath with ethyl alcohol in ultrasonic equipment. Chemical etching was performed with 2% Nital (98% solution of ethyl alcohol and 2% nitric acid).

2.2 Optical and Scanning Electron Microscopies

The cross-sectional samples were analyzed using optical microscopy (OM) and scanning electron microscopy (SEM), as well as x-ray energy-dispersive spectroscopy (EDX). SEM analyses were performed in the secondary electron and backscattered electron modes. Analysis of EDX by x-rays, spot and in-line scanning (perpendicular to the growth of the layer and toward the substrate) were performed to qualitatively determine the compositions of the formed layers.

2.3 Hardness Tests

Two types of hardness tests were performed, Brinell hardness on cast iron substrates and Vickers microhardness on the carbide layers. In both cases, a total of 20 measurements were made on each material to obtain the mean and standard deviations.

To obtain the average hardness of the layers and microhardness profiles (layer/substrate), a load of 0.5 N with an indentation time of 15 s were used. For the microhardness profiles, the first indentation was performed on the top of the layer (surface), identified in the graph with the distance 0 (zero) on the x-axis. The second and third indentations were performed on the cross section of the layer. The fourth indentation was carried out in the sublayer. The other indentations were performed on the substrate.

2.4 X-ray Diffraction

To characterize the phases and compounds formed on the samples x-ray diffraction (XRD) analyses were used on the layers and on the substrate. A x-ray tube with a Cu target yielding a $K\alpha 1 = 1.5405$ Å and a graphite monochromator were used. Two scanning speeds were used, a normal mode (2°/min − 2θ ranging from 20 to 110°) on the substrate and the incidence mode (1°/min − 2θ ranging from 20 to 120°) for the layers.

The diffractograms obtained for the substrates were plotted on separate graphs for better visualization of the peaks with their respective intensities. The patterns obtained for the layers produced were plotted with relative intensities in reference to the most intense peak of each diffractogram making it possible to compare the layers with the same composition for different substrates.

Table 2 Chemical compositions of ferro-alloys and aluminum used in TRD treatment baths (wt%)

| Material | Chemical element, wt.% | | | | |
	Al	Nb	V	Fe	Si
Aluminum	97.9	…	…	…	2.1
Ferro-niobium	…	73.4	…	23.9	2.7
Ferro-vanadium	…	…	56.6	40.6	2.8

Table 1 Chemical compositions of ductile cast iron (wt.%)

| Ductile cast irons | Chemical elements, wt.% | | | | | | |
	C	Si	Mn	Cu	Ni	Mo	Fe
Unalloyed	4.35	2.59	0.15	…	…	…	Bal
Alloyed with Cu	3.71	2.69	0.22	0.69	…	…	Bal
Alloyed with Cu-Ni	3.73	2.65	0.22	0.68	1.24	…	Bal
Alloyed with Cu-Ni-Mo	3.78	2.56	0.25	0.69	1.69	0.27	Bal

2.5 Adhesiveness Tests of Layers—VDI 3198

Daimler-Benz Rockwell C layer adhesion tests described in VDI 3198 (*Verein Deutscher Ingenieure Normen*) were performed (Ref 13, 14). Five Rockwell indents were applied on each of the carbide layer surfaces which were subsequently evaluated by means of OM.

2.6 Micro-Adhesive Wear Tests

The Calotest wear test was used to evaluate the adhesive wear resistance of both the substrate and the layers. As described in (Ref 3, 15), this test utilizes a fixed steel ball of AISI 52,100 steel with a diameter of 25.4 mm and a hardness of 61 HRC. The ball rotates at 400 RPM sliding against the sample with a force of 8.7 N and the data, volume removed against sliding distance, is used to obtain the wear curves. In order to characterize the variability of the process three tests were performed on each sample and the average volumes removed and respective standard deviation were calculated. The ambient conditions were 27.5 °C and 55% relative humidity. After the conclusion of each sliding distance, the concave spherical cap was measured and the worn volume was calculated according to Eq 1:

$$V = \frac{\pi d^4}{64R} \text{ for : } d << R \qquad \text{(Eq 1)}$$

where V: volume removed; d: diameter of the cap and R: 12.7 mm (radius of the sphere) (Ref 3, 15).

3. Results and Discussion

3.1 Characterization of the Cross Sections of the Layers Produced

Figure 1 and 2 shows the optical micrographs of the cross sections of the layers produced by TRD treatment followed by air-cooling or direct-austempering. There are three regions: I. Carbide layer, II. interface and III. the substrate. The formation of this sublayer at the interface, as reported previously for steels, consists of iron and chromium or double-layers composed of the diffusion sublayer and chromium carbide on the surface of the layer produced (Ref 8).

The carbide layers obtained in steels by means of TRD treatment are formed in three stages: (1) Primary nucleation and growth of grains smaller than 0.1 μm, (2) carbide generation and interconnection of grains and (3) growth of the carbide layer by successive diffusion during the treatment. Since the characteristics of the carbide layers produced in ductile cast irons are similar to those obtained in steels, suggest that the mechanisms of formation and growth of the layers are also similar (Ref 8, 16).

For TRD treatments followed by air-cooling, the substrates of ductile cast irons without alloying and alloyed with Cu showed a pearlitic matrix. For the ductile cast iron alloyed with Cu-Ni, a mixed matrix of pearlite and ausferrite was obtained (shown in Fig. 1 and 2 with yellow arrows), indicating that the addition of Ni increased the austemperability of the material for the treatment condition used. In the case of cast iron alloyed with Cu-Ni-Mo, the matrix showed a fully ausferritic microstructure due to its greater austemperability making it possible to obtain such microstructure without the need for treatment in a salt bath.

In the case of TRD treatments followed by austempering, the unalloyed ductile cast iron showed a mixed matrix of pearlite (shown in Fig. 1 and 2 with the red arrows) and ausferrite. The partial microstructural transformation of this substrate may be associated with borax dragout from the TRD treatment bath to the austempering bath. After TRD treatment, the sample was removed from the borax bath and transferred directly to the austempering bath. In this procedure, the sample adds its residual surface borax, which may have hindered complete transformation to ausferrite due to the resulting isolation. For ductile cast irons with the addition of alloy elements, ausferritic microstructures were produced.

The addition of alloying elements also influenced the acicular ferrite of the austempered substrates. Cu alloyed ductile cast iron showed a more refined microstructure when compared to Cu-Ni-Mo alloyed ductile cast iron. This is because the lower the amount of alloying elements in the material, the greater the cooling of the austenite and the lower the rate of carbon diffusion, favoring nucleation of the more refined acicular ferrite. The opposite effect occurs for compositions with a greater amount of alloying where the rate of carbon diffusion is higher, resulting in the development of coarse ausferrite (Ref 3).

The average hardness of the substrates is shown in Table 3.

The addition of alloying elements in the ductile cast irons increased substrate hardness. Cu-Ni-Mo alloyed ADI showed the highest hardness value, followed by Cu-Ni and Cu-alloyed ADIs, respectively. For unalloyed ductile cast iron, in the untreated or austempered condition, no significant hardness variation was observed which confirms that the material was partially austempered.

Uniform layers were produced by the TRD treatment without the presence of graphite nodules together with a flat interface with the substrate. Similar layers have been produced in works published in the literature in the case of TRD treatment in steels (Ref 10, 11, 17-19). The average thicknesses of the layers produced are shown in Table 4.

Table 3 Results of Brinell hardness tests (HB) for untreated and austempered ductile cast irons

Ductile cast irons	Not treated	Austempered
Unalloyed	214 ± 2	218 ± 5
Alloyed with Cu	242 ± 3	337 ± 7
Alloyed with Cu-Ni	266 ± 4	349 ± 9
Alloyed with Cu-Ni-Mo	313 ± 15	415 ± 8

Table 4 Average layer thickness and their respective standard deviations produced on the ductile cast iron using the TRD treatment

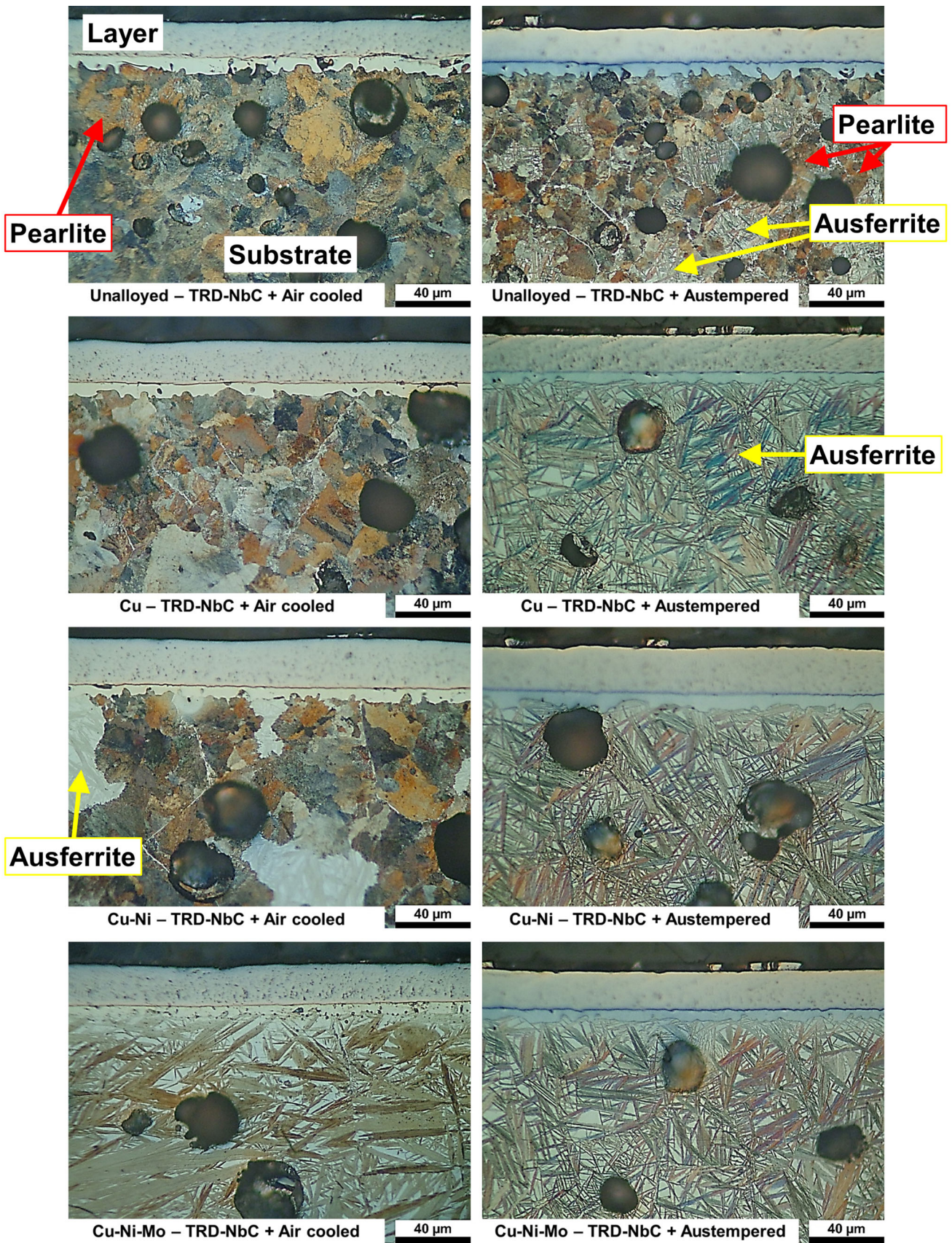| Ductile cast irons | Layer thicknesses, μm | |
	TRD-NbC	TRD-VC
Unalloyed	17.8 ± 0.4	15.4 ± 0.4
Alloyed with Cu	21.5 ± 0.8	18.5 ± 1.3
Alloyed with Cu-Ni	23.1 ± 0.6	19.1 ± 1.7
Alloyed with Cu-Ni-Mo	20.0 ± 0.9	17.9 ± 0.6

Fig. 1 Optical micrographs of the cross sections of the ductile cast irons after TRD-NbC treatment. Red and yellow arrows indicate the pearlite and ausferrite microstructures, respectively (Color figure online)
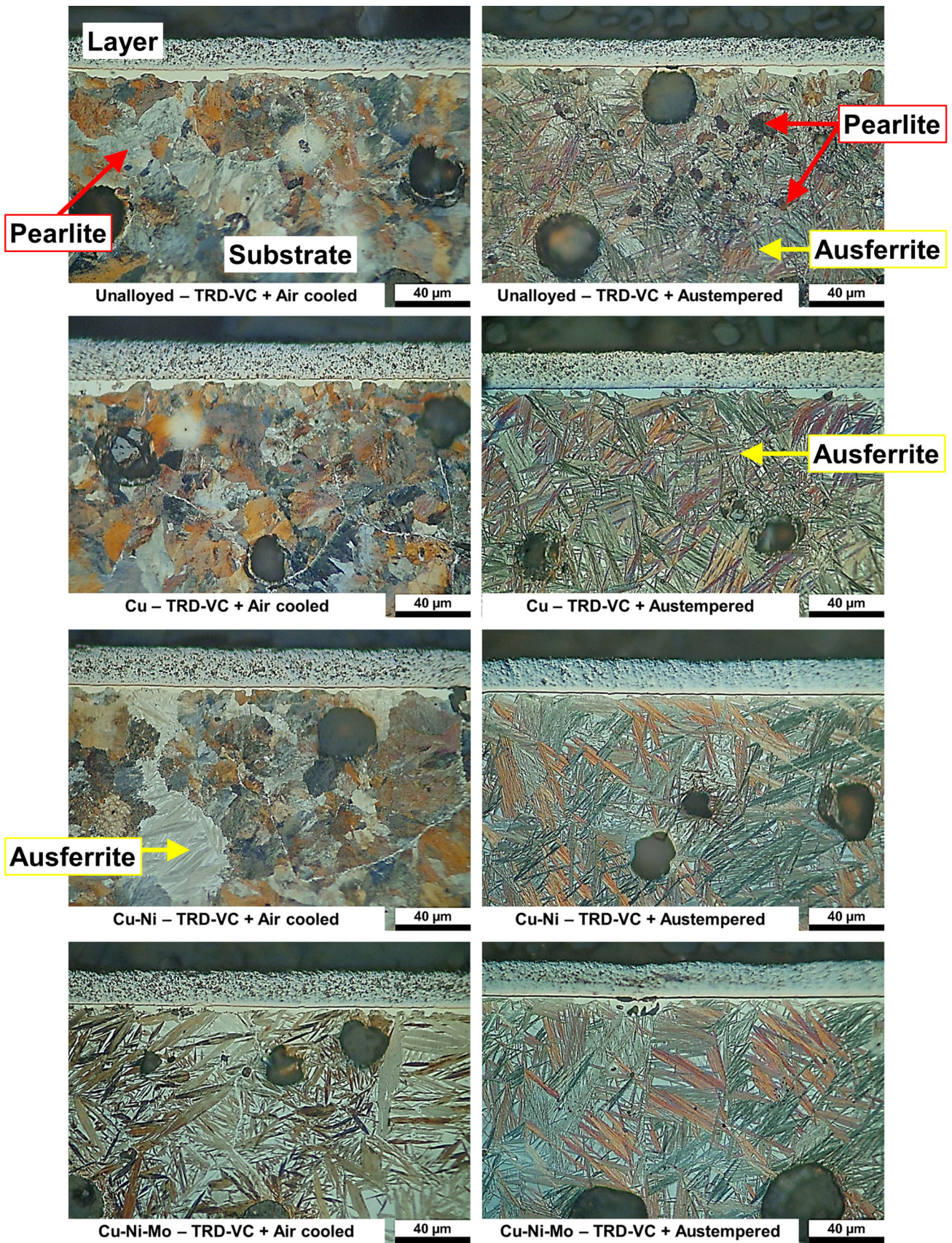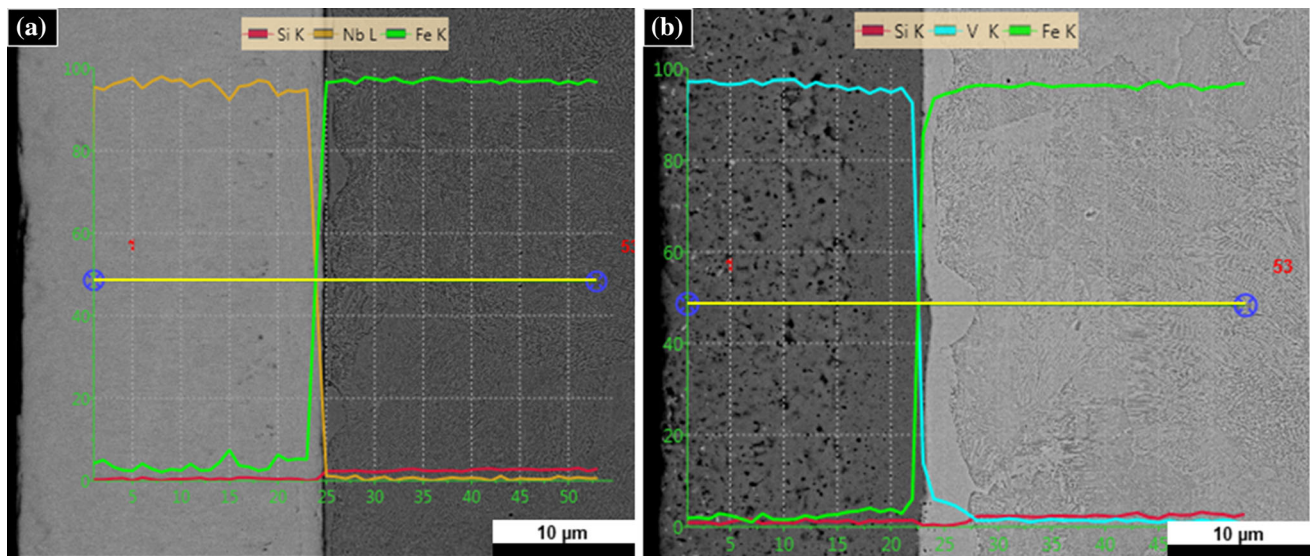
Fig. 2 Optical micrographs of the cross sections of the ductile cast irons after TRD-VC treatment. Red and yellow arrows indicate the pearlite and ausferrite microstructures, respectively (Color figure online)

Fig. 3 EDX in line with the cross section of the ductile cast iron alloyed with Cu: (a) TRD-NbC and (b) TRD-VC

The thicknesses of the carbide layers obtained in the ductile cast irons were greater than those obtained in steels treated under similar conditions in previous works that were published in the literature (Ref 10, 12, 17, 20). It is observed that the unalloyed ductile cast iron showed the lowest carbide layer thickness and that the addition of the alloying elements increased the layer thicknesses. It appears that the addition of molybdenum produced a decrease in layer thickness when compared to Cu-Ni ADI sample. This behavior had already been observed in another study in which vanadium carbide layers were produced in two compositions of Cr12MoV steel, varying only the proportion of molybdenum (Ref 21).

This is due to the influence of the added elements on the carbon diffusivity. Austenite stabilizing elements (Cu and Ni) increase carbon diffusivity while carbide-forming elements decrease it (Mo). Empirical equations were developed to predict the diffusivity of carbon in austenite as a function of chemical composition and temperature, as shown in Eq 2 (Ref 22).

$$D(T, M, C) = \left[0, 1460, 036 \cdot C \cdot (1 - 1075.Cr) \sum k_1 M\right]$$
$$\cdot \exp\left(-\frac{1443 - 150.C + 037 \cdot C^2 + \sum k_2 M}{R_{kj} \cdot T}\right)$$
(Eq 2)

where C is the weight percentage of carbon, R_{kJ} is the gas constant (kJ/mol-K); T is the absolute temperature (K); M is the weight percentage for each alloying element and; k_1 and k_2: are the parameters of diffusivity coefficient and energy of activation of carbon in austenite, respectively, for each alloy element.

In Fig. 3, the scanning electron micrographs of the carbide layer cross sections produced in the ductile cast iron with Cu are shown together with the EDX analysis by x-rays in line from the surface of the layer toward the center of the substrate. TRD-NbC (Fig. 3a) and TRD-VC (Fig. 3b) treatments were followed by air-cooling.

The layers produced showed high levels of the carbide-forming elements (niobium or vanadium) added to the salt baths, indicating the formation of carbide layers. In the layer/substrate interface, there is a marked decrease in both elements, together with a large increase in the iron content, indicating the formation of layers with flat and well-defined interfaces without the occurrence of diffusion of the carbide forming elements into the substrate or from the iron and silicon of the substrate into the layer.

The results of EDX in-line at the cross section obtained in the cast iron alloyed with Cu were similar to those found in steels treated under similar conditions in previous works that were performed and in the literature (Ref 10, 12, 17, 21).

Figure 4 shows the SEM and EDX analyses for each region (layer, sublayer and substrate) obtained from the ductile cast iron with Cu after the TRD treatments followed by air-cooling.

The layers produced indicated the presence of carbide-forming elements Nb and V for the TRD-NbC and TRD-VC treatments, respectively. In the sublayer regions, the presence of the elements Fe from the substrate, and Cr probably from the AISI 316 stainless steel crucible used in TRD treatments is detected. EDX analyses of the TRD baths (carried out after their solidification) were performed after the treatments and are shown in Table 5.

The presence of the elements Na and O that make up the borax; Nb, V and Fe from the carbide-forming elements added to the powder baths for the production of the layers; Si from Al and ferro-alloys used, and also the presence of Cr, probably from the stainless steel crucible AISI 316 used in TRD treatments is observed. In the borax bath at 1000 °C, Cr has greater free energy for carbide formation ($-$ 13 kcal/mol) allowing diffusion to be more favorable thermodynamically, followed by V ($-$ 24 kcal/mol) and Nb ($-$ 33 kcal/mol), respectively (Ref 8, 16, 23). This favored the formation of the sublayer present in micrographs.

3.2 Vickers Microhardness Tests

Table 6 shows the Vickers microhardness values of the layers produced by the TRD treatments in the ductile cast irons.

It is observed that the TRD-NbC treatment produced layers with hardness values between 2332 and 2345 $HV_{0.5}$. ANOVA statistical analysis of the hardness shows with 99.9% reliability that the layers have, on average, the same hardness. This indicates that the variations of alloying elements added to the
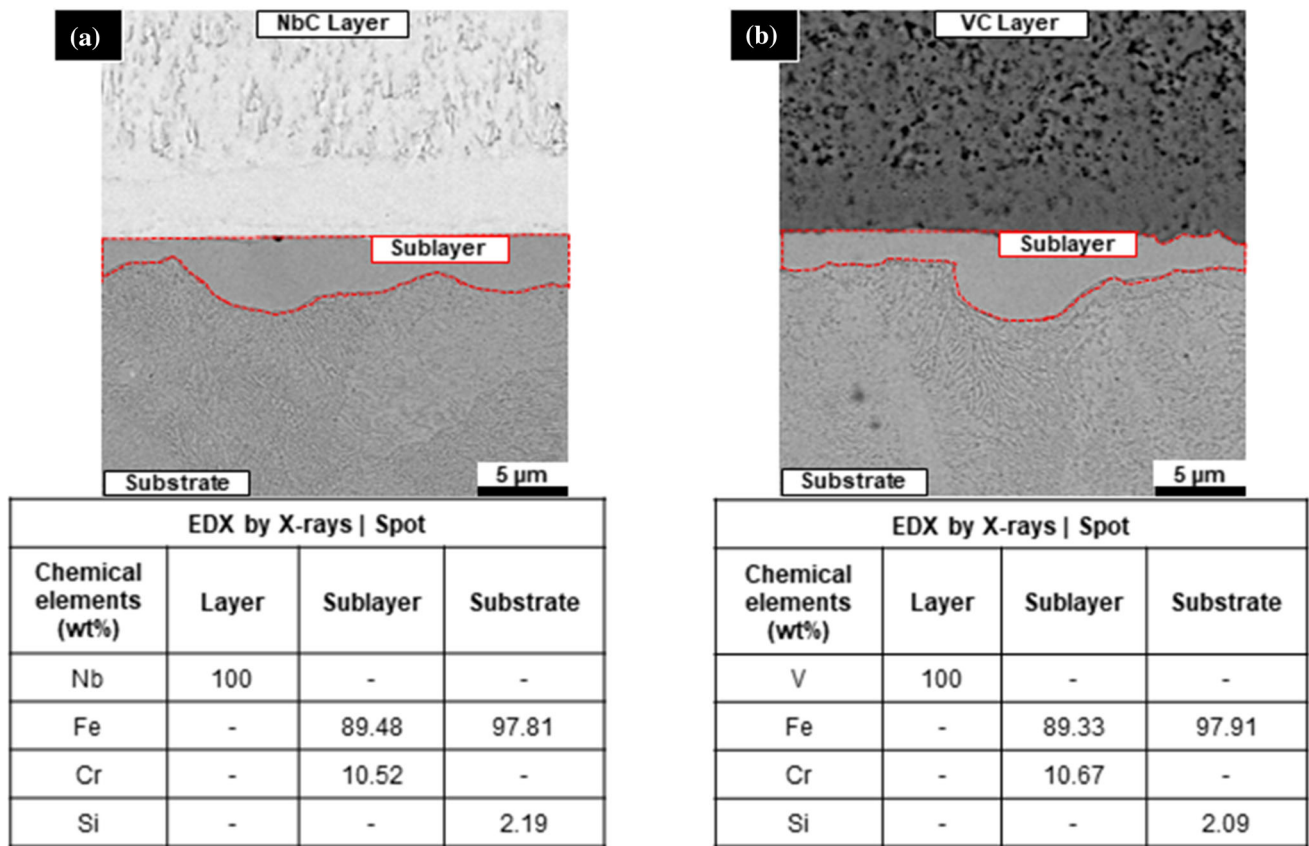
Fig. 4 SEM and EDX for each region (layer, sublayer and substrate) obtained from the Cu alloyed ductile cast iron after treatments (a) TRD-Nb and (b) TRD-V, followed by air-cooling

Table 5 EDX of the baths of TRD treatments

TRD treatment	Elements contained in the bath, wt.%							
	O	Na	Al	Nb	V	Fe	Cr	Si
TRD-NbC	51.3	28.0	3.6	6.7	…	7.7	1.8	0.9
TRD-VC	54.6	27.4	4.9	…	5.1	5.6	1.7	0.7

ductile cast irons did not influence the hardness of the layers produced. The hardness levels obtained for the niobium carbide layers in all cast iron samples were similar to those obtained in the TRD-NbC treatments in AISI H13, M2 and D2 steel according to (Ref 9, 18, 24), and for the AISI steel L2 (Ref 25).

The TRD-VC treatment produced layers with hardness values between 2533 and 2557 $HV_{0.5}$. As observed for the layers produced using the TRD-NbC treatment, the TRD-VC treatment produced layers with similar average hardness, with ANOVA statistical analysis indicating 99.9% reliability. These results support the premise that the carbide layers produced (NbC or VC) have similar hardness. Therefore, it can be confirmed that the variations of alloying elements added in the chemical compositions of the substrates studied did not influence the hardness of the layers produced. The levels of hardness obtained for the layers in all the cast iron samples were similar to those obtained in layers of vanadium carbide produced in AISI D2 steels according to (Ref 18, 20) and for Cr12MoV steel (Ref 26).
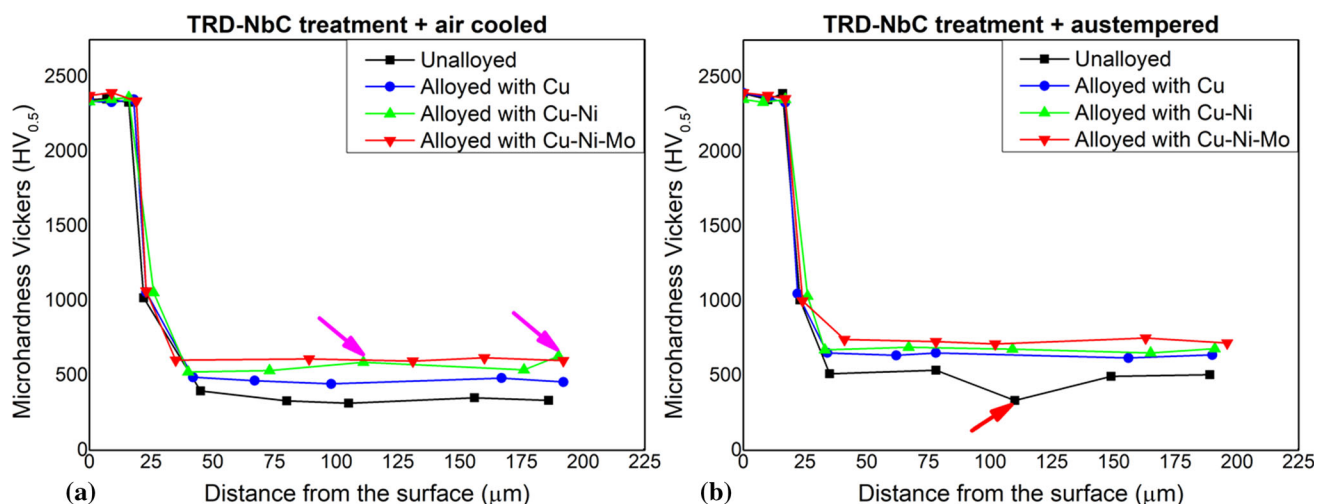
The Vickers microhardness profiles for the carbide layers and substrates of cast iron are shown in Fig. 5 and 6.

The microhardness profiles obtained in the cross sections were similar for all TRD treatments maintaining a constant layer hardness throughout. At the layer/substrate interface, the formation of a sublayer is observed with hardness in the range of 1000 and 1100 $HV_{0.5}$. The hardness of the substrates remained constant close to the interfaces indicating that there was no decarburization due to the carbon supply of the substrate for the formation of the layer. The microhardness profiles obtained for the carbide layers produced in cast iron were similar to those obtained in steel treated under similar conditions as reported in previous works that were published in the literature (Ref 10).

For the Cu-Ni ductile cast iron substrate, the TRD treatment followed by air-cooling produced a substrate with increased hardness close to 750 $HV_{0.5}$ (indicated with the pink arrow). This value is correlated with the ausferritic microstructure obtained during cooling in air, as seen in Fig. 1. In the case of unalloyed ductile cast iron, TRD treatment followed by direct

Table 6 Vickers microhardness (HV) results for the layers produced by the TRD treatments in ductile cast irons

Ductile cast irons	TRD-NbC		TRD-VC	
	Air cooled	Austempered	Air cooled	Austempered
Unalloyed	2341 ± 139	2332 ± 136	2540 ± 115	2539 ± 64
Alloyed with Cu	2339 ± 98	2345 ± 90	2533 ± 60	2546 ± 55
Alloyed with Cu-Ni	2342 ± 113	2344 ± 140	2557 ± 75	2553 ± 82
Alloyed with Cu-Ni-Mo	2333 ± 131	2335 ± 129	2534 ± 83	2544 ± 57
Load 0.5 N				

Fig. 5 Vickers microhardness profiles obtained for the niobium carbide layers. (a) TRD + air cooling and (b) TRD + austempering. The pink and red arrows indicate the hardness obtained for the ausferritic and pearlitic phases, respectively (Color figure online)

austempering produced a decrease in hardness as is noted in the substrate region indicated with the red arrow. This value, close to 250 $HV_{0.5}$, refers to the pearlitic region resulting from the incomplete transformation of primary austenite into ausferrite, as seen in Fig. 1.

3.3 X-ray Diffraction

The resulting XRD diffractograms of the sample's substrates without alloying and alloyed with Cu, Cu-Ni and Cu-Ni-Mo, are shown in Fig. 7.

There is only the presence of the α (ferrite) and γ (austenite) phases, indicating that the treatment window has not been exceeded, since if this had occurred, the ε (Fe_3C) phase would appear due to austenite decomposition. The same phases were observed in other studies with austempered ductile cast irons where the ausferritic microstructure was obtained (Ref 27, 28).

Figure 8 shows the diffractograms of the layers produced with the TRD treatments, followed by direct austempering for the ductile cast irons alloyed with Cu, Cu-Ni and Cu-Ni-Mo, respectively.

In Fig. 8a, is indicated only niobium carbide (NbC) with a cubic structure in all cases, confirmed according to the crystallographic sheet ID 20,073, showing high intensity peaks with a mixed orientation of the crystallographic planes (111), (200), (220), (222), (311), (331), (400), (420) and (422). Niobium carbide has a cubic crystalline system similar to NaCl (Fm-3 m) and falls under the spatial group number 225 (Ref 29). The phase obtained in the layers produced in the cast irons

is in agreement with those obtained in the literature for similarly treated steels (Ref 9, 11, 18, 24).

In Fig. 8b, the presence of only vanadium carbide (VC) resulting from the treatment is verified. The VC cubic phase was confirmed according to the crystallographic sheet ID 33,478, showing high intensity peaks with a mixed orientation of the crystallographic planes (111), (200), (220), (222), (311), (331), (400) and (420). Vanadium carbide also has a cubic crystalline system similar to NaCl (Fm-3 m) and falls under the space group number 225 (Ref 29). No significant effect of the composition of the borax bath or the substrate was observed in the present guidelines. The x-ray diffraction spectra obtained are consistent with those found in the literature for similarly treated steels (Ref 17, 18).

3.4 Layer Adhesion Tests—Daimler-Benz VDI 3198

Figure 9 and 10 shows the optical micrographs obtained for Rockwell C indentations on the surfaces of ductile cast irons samples after TRD treatments.

There are some microcracks (indicated with the yellow arrow) and delamination (indicated with the red arrow) acceptable with the standards established for the test standard VDI 3198 which can be referred to as classes HF1 and HF3 (Ref 13, 14). This affirms that the layers produced through the TRD treatments followed by air-cooling or direct austempering in ductile cast irons showed good adhesion to the substrate. Similar layers were produced in previous works according to the literature (Ref 13, 14).
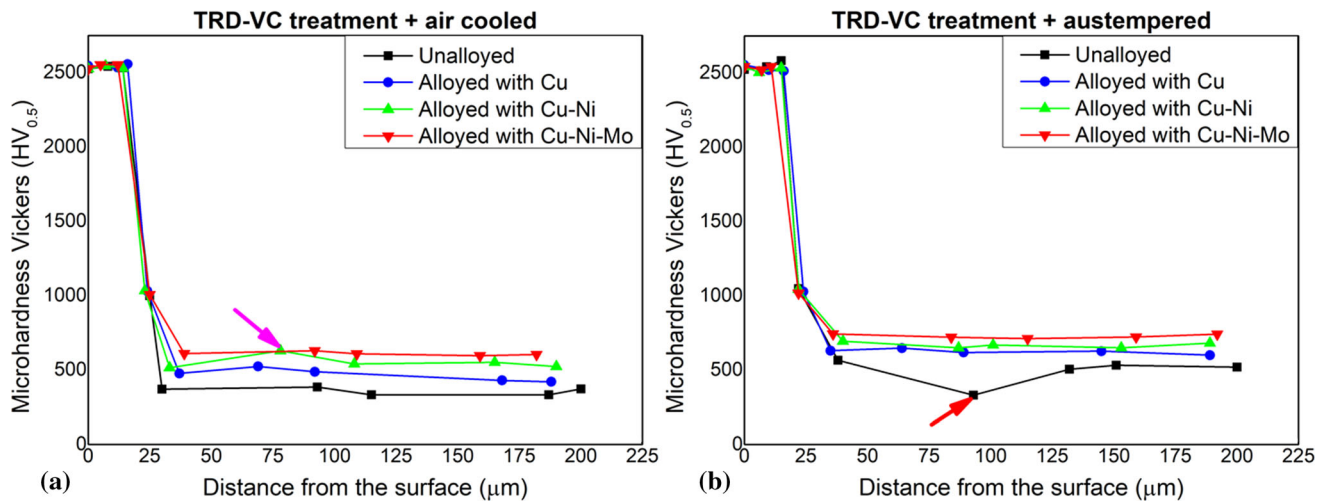
Fig. 6 Vickers microhardness profiles obtained for the vanadium carbide layers. (a) TRD + air cooling and (b) TRD + austempering. The pink and red arrows indicate the hardness obtained for the ausferritic and pearlitic phases, respectively (Color figure online)
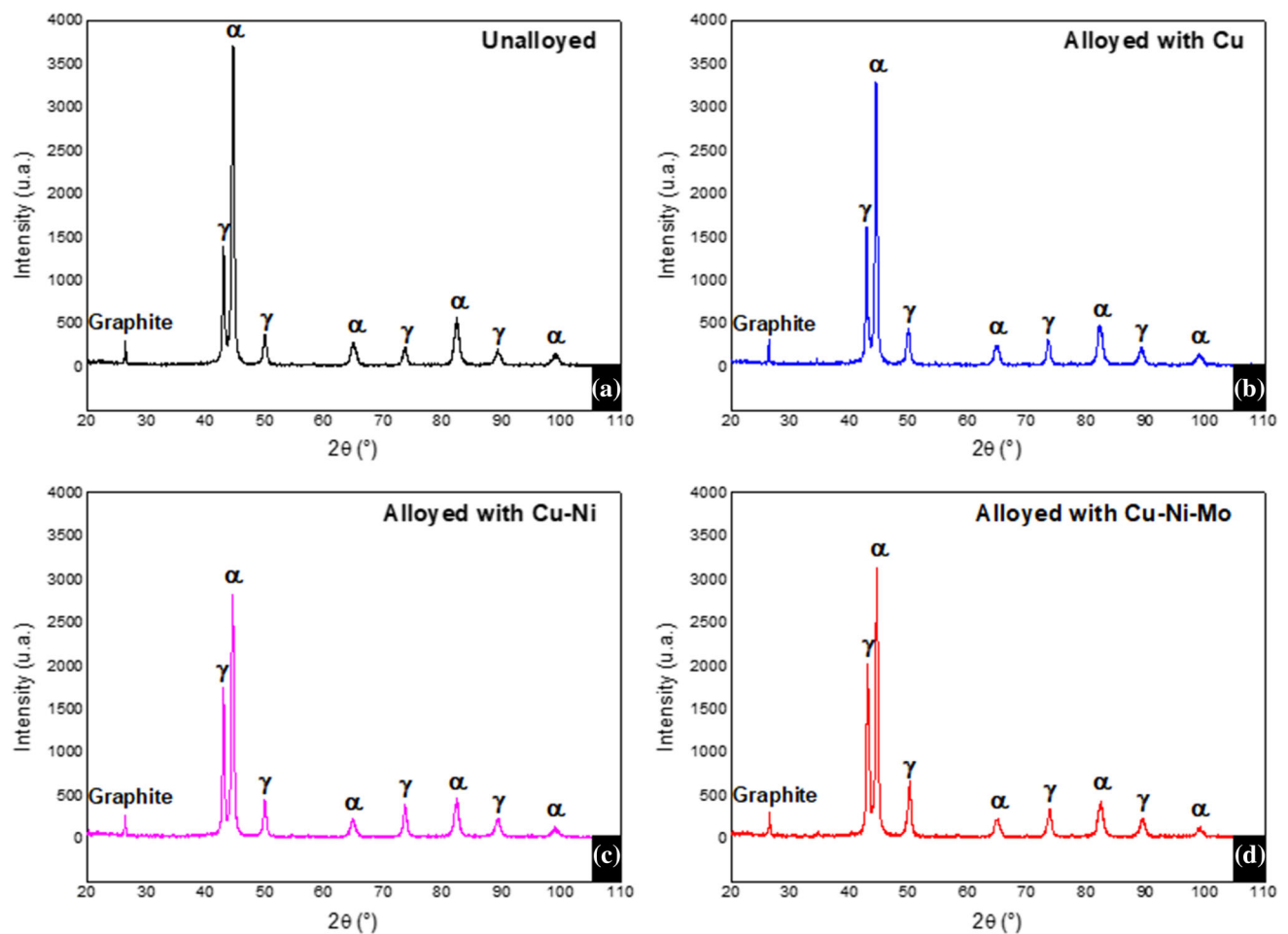

Fig. 7 Diffractograms of TRD treated ADI substrate samples. (a) Unalloyed and alloyed with (b) Cu, (c) Cu-Ni and (d) Cu-Ni-Mo

3.5 Micro-Adhesive Wear Tests

The results of the micro-adhesive wear tests for austemperated ductile cast irons are presented together with the carbide layers produced by the TRD treatments (Fig. 11).

Austempered cast irons showed lower resistance to adhesive wear when compared to samples with carbide layers. Among the austempered substrates, the Cu-Ni-Mo ductile cast iron exhibited the greatest wear resistance, followed by the Cu-Ni
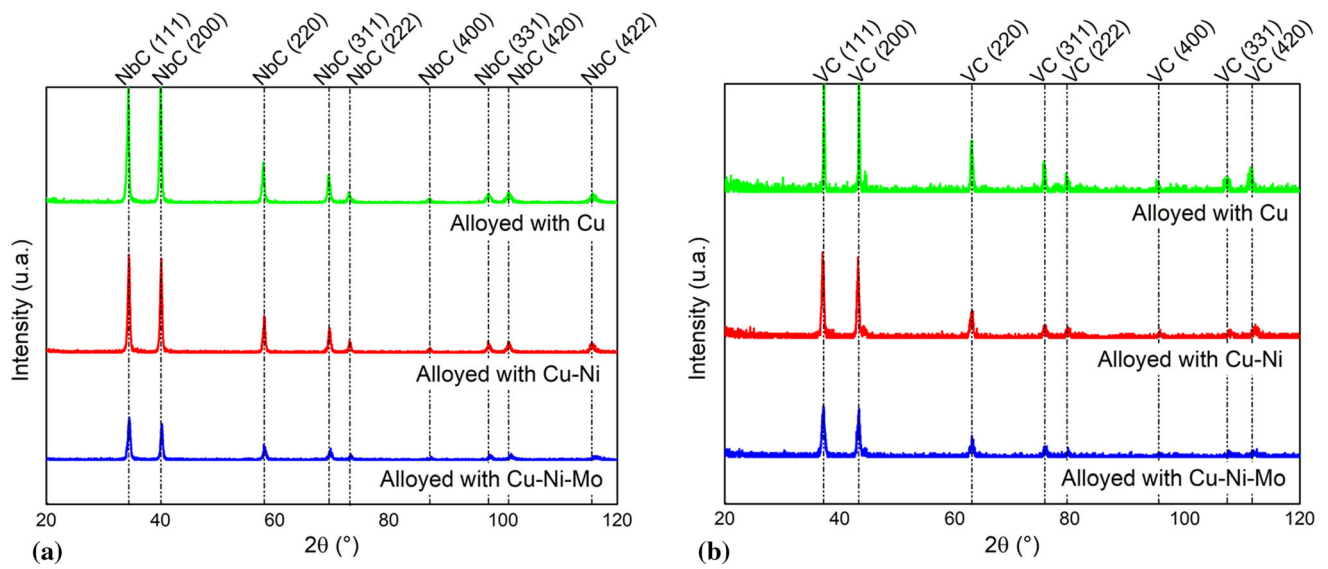
Fig. 8 Diffractograms of the layers obtained in the ductile cast iron alloyed with Cu, Cu-Ni or Cu-Ni-Mo. (a) TRD-NbC and (b) TRD-VC treatments
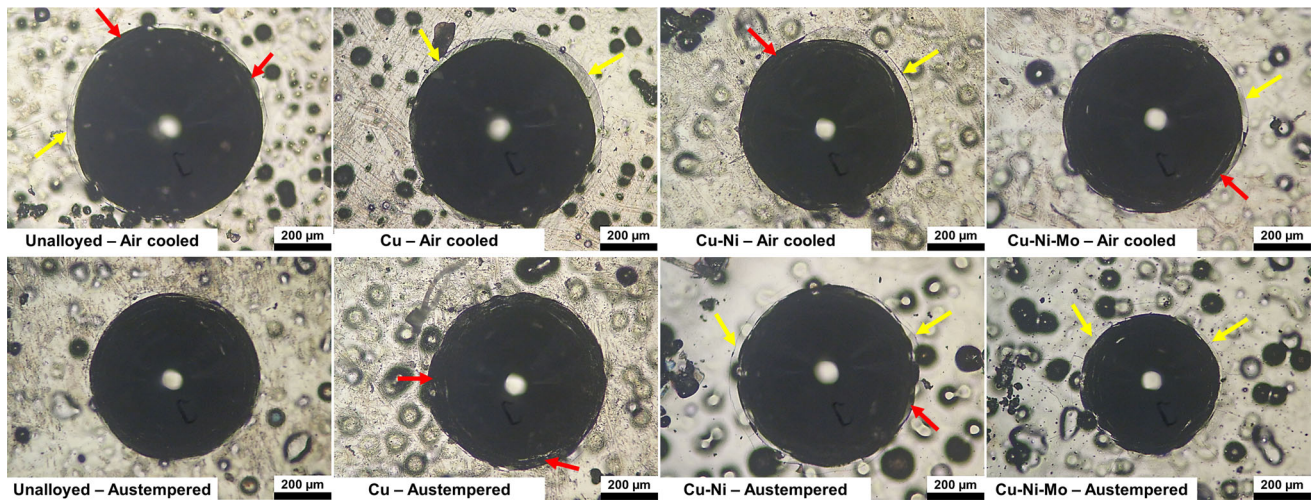

Fig. 9 Rockwell C indentations on the surfaces of ductile cast irons. TRD-NbC treatments
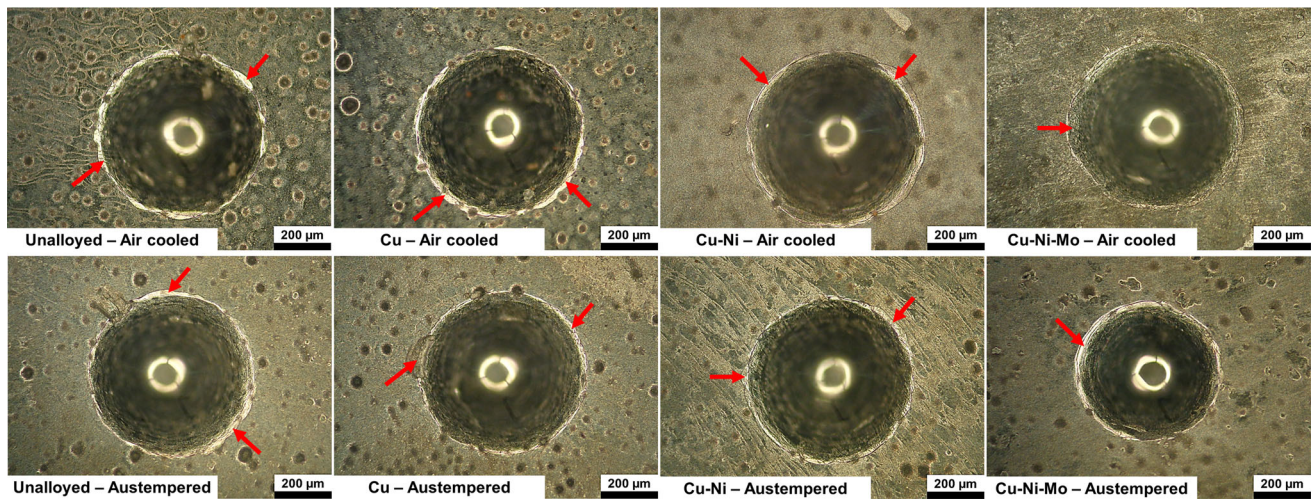

Fig. 10 Rockwell C indentations on the surfaces of ductile cast irons. TRD-VC treatments
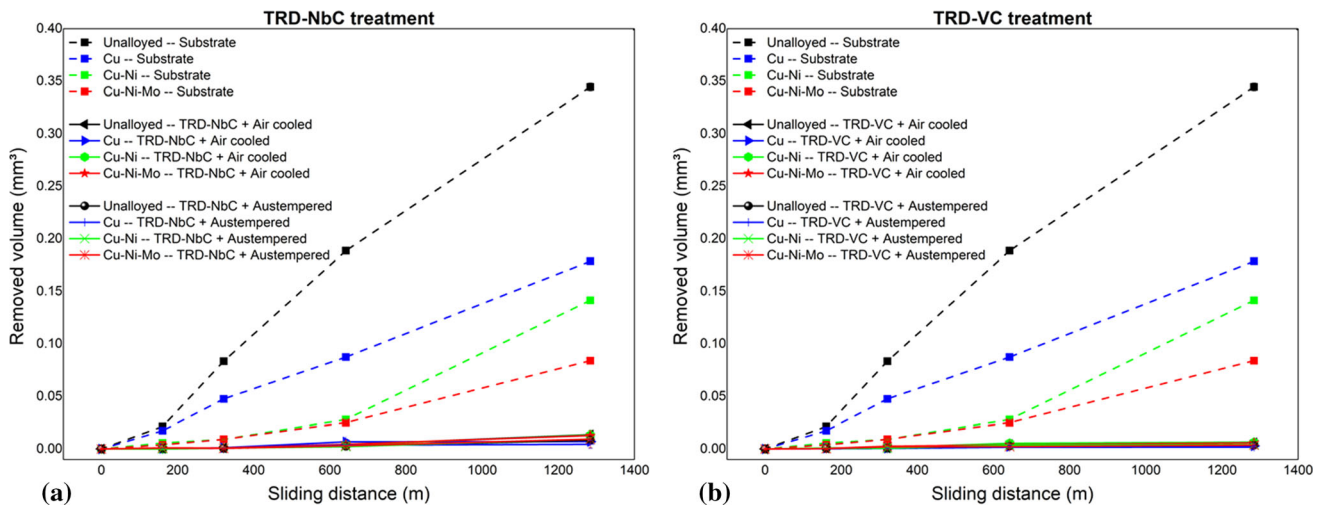
Fig. 11 Micro-adhesive wear tests: (a) TRD-NbC and (b) TRD-VC treatments

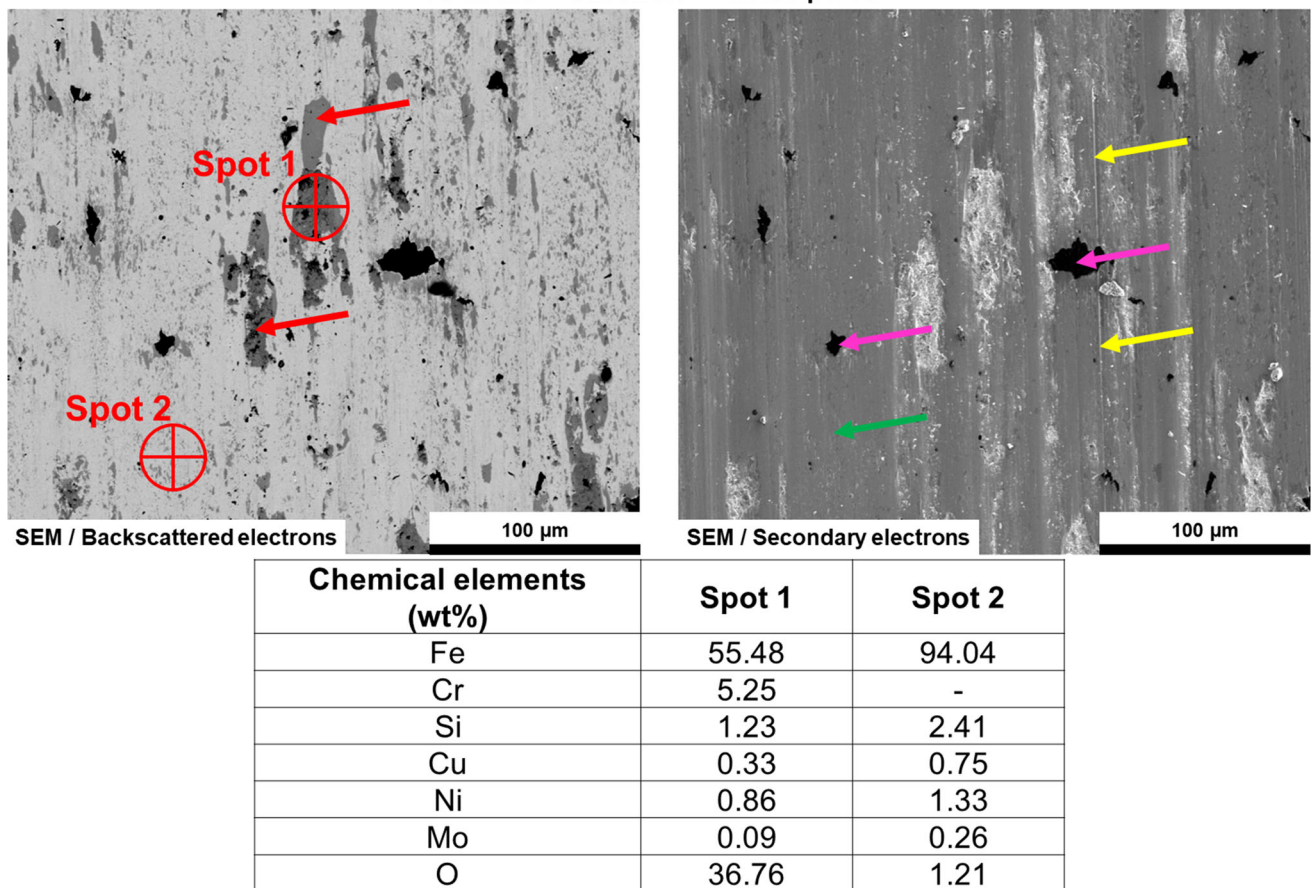| Chemical elements (wt%)	Spot 1	Spot 2
Fe	55.48	94.04
Cr	5.25	-
Si	1.23	2.41
Cu	0.33	0.75
Ni	0.86	1.33
Mo	0.09	0.26
O	36.76	1.21

Fig. 12 Scanning electron micrographs of the interior of the wear cap of the austempered Cu-Ni-Mo ductile cast iron, along with region EDX analyzes. The red, yellow and green arrows indicate the mechanisms of adhesive and abrasive wear on two and three bodies, respectively. The pink arrow indicates detachment of the material during the wear test (Color figure online)

ductile cast iron, Cu and unalloyed ductile cast iron. Among ductile cast irons, the addition of alloying elements provided increases in hardness values, as shown in Table 3. This increase in hardness can be associated with increased wear resistance, indicating that the addition of alloy elements can improve the wear resistance of austempered ductile cast irons.

The carbide layers produced by means of TRD treatments, yielded similar wear resistance, up to 35 times greater when compared to ductile cast iron unalloyed and 5 times greater when compared to Cu-Ni-Mo.

Normally, wear resistance of materials is associated with their hardness and is inversely proportional according to the

Cu-Ni-Mo – TRD-NbC - Austempered

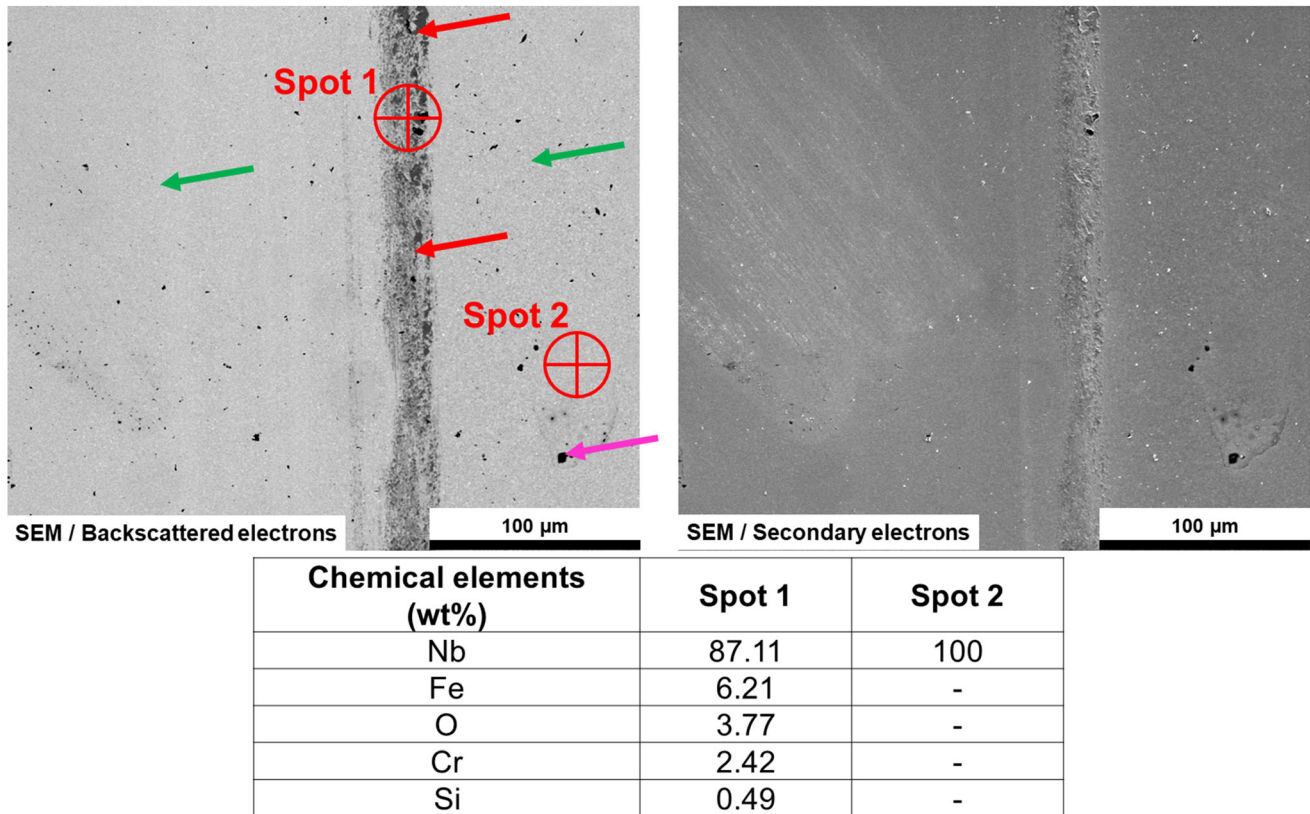| Chemical elements (wt%)	Spot 1	Spot 2
Nb	87.11	100
Fe	6.21	-
O	3.77	-
Cr	2.42	-
Si	0.49	-

Fig. 13 Scanning electron micrographs of the interior of the wear caps from the NbC layer, together with the analysis of EDX by region. The red and green arrows indicate the mechanisms of adhesive and abrasive wear on tree bodies, respectively. The pink arrow indicates detachment of the material during the wear test (Color figure online)

Archard equation (Eq 3). There are articles in the literature that indicate use of the Archard for the evaluation of carbide layer wear. The Archard equation provides an empirical correlation between the wear volume removed and the hardness of the material. Where, V: volume removed; k: is the wear coefficient; L: is the applied load; D: is the sliding distance and; H: is the hardness of the material (Ref 30).

$$V = k\left(\frac{L \cdot D}{H}\right) \qquad \text{(Eq 3)}$$

Among the TRD treatments followed by air-cooling and direct austempering, it is observed that austempering did not influence the wear resistance of the layers as observed in their hardness.

Figure 12 shows the scanning electron micrographs of the interior of the cap obtained for the longest sliding distance (test time 40 min-1280 m sliding distance), together with point EDX analyzes, for the ductile cast iron substrate Cu-Ni-Mo.

It is observed that the active wear mechanisms on the substrates are adhesive, characterized by the presence of transfer films (indicated by red arrows), and the abrasive mechanisms on two bodies, characterized by scratches and directional grooves (indicated by yellow arrows), and three bodies, smooth region (indicated by green arrows). The abrasive responsible was probably the chromium carbide from the sphere (AISI 52,100), which stood out and subsequently adhered to it. Through the point x-rays EDX analysis of the transfer film (Spot 1), the presence of Fe, O and Cr is verified,

indicating that such films are made up of oxides of these metals, which came from the steel sphere AISI 52,100 used in the wear test. The presence of Si, Cu, Ni and Mo is attributed to the chemical composition of the ductile cast iron. In the EDX Spot 2 analysis, values were obtained with chemical compositions similar to those of the ductile cast iron Cu-Ni-Mo (Table 1), indicating abrasive wear. Similar wear mechanisms have been obtained in previous works that we performed (Ref 3).

Scanning electron micrographs of the interiors of the caps obtained for the layers of NbC (Fig. 13) and VC (Fig. 14), produced on the ductile cast iron substrate Cu-Ni-Mo are presented together with the specific EDX analyses. The analyzed caps refer to the longest sliding distance (test time 40 min-1280 m sliding distance).

In Fig. 13, it can be seen that in Spot 1 there was a transfer of metallic film from the sphere used in the test (indicated by red arrows), the presence of Fe, O, Cr and Si is noted, indicating that such films are constituted of oxides of these metals, which came from the AISI 52,100 steel ball used in the wear test. In Spot 2, only Nb, the layer-forming element, was obtained. The wear cap also has polished regions (indicated by green arrows), indicating an abrasive wear mechanism for three bodies. Such abrasive particles are probably due to material detached from the layer.

In Fig. 14, it can be seen that there were two active wear mechanisms. The first was the adhesive mechanism, characterized by the presence of transfer films (indicated by red arrows). Through the analysis of EDX in Spot 1, the presence of Fe, O,
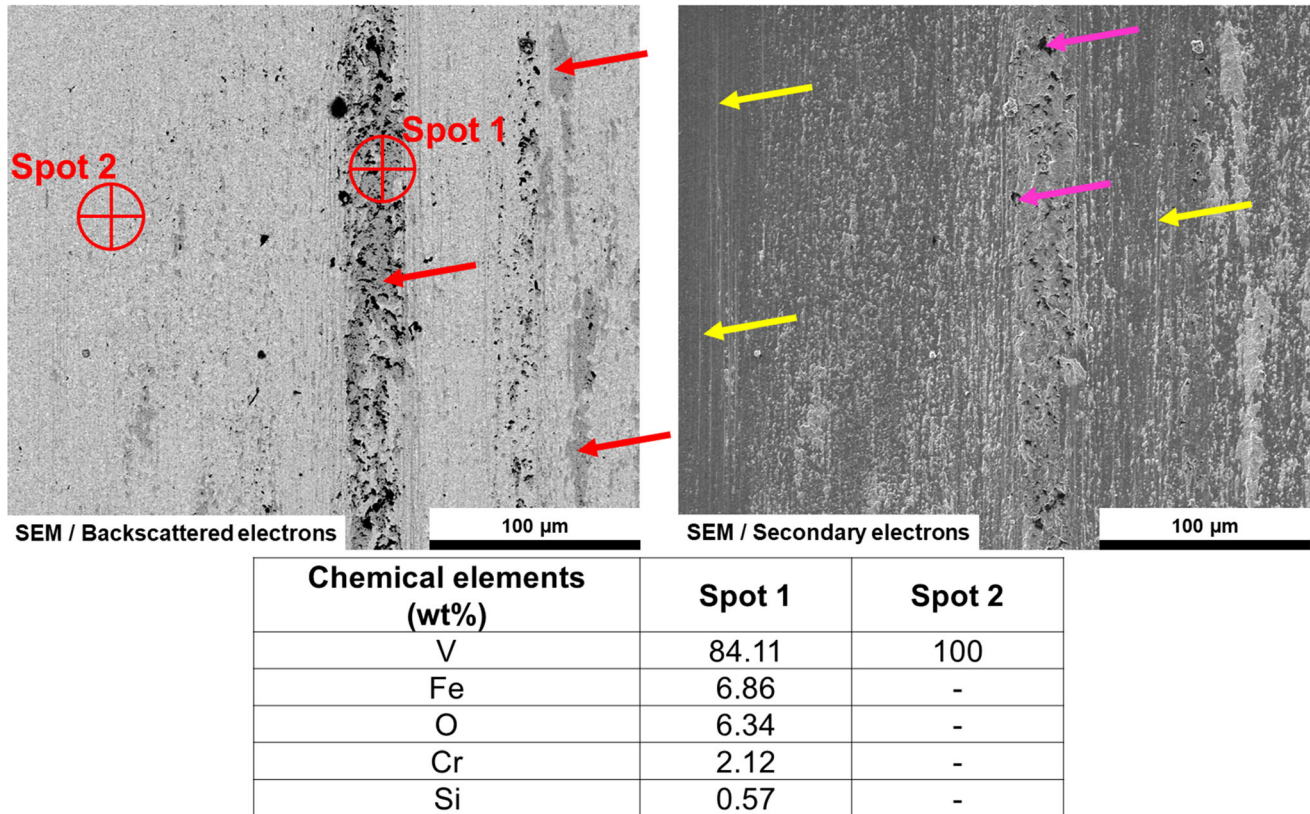
Fig. 14 Scanning electron micrographs of the interior of the wear caps from the VC layer, together with the analysis of EDX by region. The red and yellow arrows indicate the mechanisms of adhesive and abrasive wear on two bodies, respectively. The pink arrow indicates detachment of the material during the wear test (Color figure online)

Cr and Si is verified, indicating that such films are constituted of oxides of these metals, which came from the sphere used in the wear test. The second was two-body abrasive type, characterized by directional scratches (indicated by yellow arrows). Through the analysis of EDX in Spot 2, only the V, which forms the layer, was detected. There are also directional risks (indicated by yellow arrows), which is indicative of two bodies abrasive wear. The abrasive mechanism of these layers is probably the result of the particle detachment during wear which can adhere to the sphere and act as an abrasive.

The wear mechanisms obtained for the wear caps in the carbide layers presented characteristics similar to those obtained in previous works that were published in the literature (Ref 18).

4. Conclusions

The alloying used on the ductile iron samples increased the hardness and wear resistance in all instances when compared to the unalloyed substrate. The austempered treatment further improved hardness.

The achieved hardness among the austempered alloyed samples, up to 750 HV, is even more impressive when no quenching was used imparting low internal stress and low distortion to the fabricated part, together with a good toughness typical of ADIs. Interestingly, alloying improved the TRD treatments while increasing the substrate performance.

The carbide layers produced by the TRD treatments showed high hardness, uniform and with excellent adhesion to the substrates. Among the ductile cast irons, the unalloyed sample showed the lowest thickness values for the carbide layers produced. The layer thicknesses increased with the addition of the Cu and Cu-Ni alloying elements, while the alloy with Cu-Ni-Mo showed a decrease proving that the addition of Mo is detrimental for layer thickness.

All the carbide layers produced showed similar wear performances, which were much higher (5 to 35 times) than the substrates in all treatment conditions.

References

1. X. Su, S. Zhao, H. Sun, X. Yang, P. Zhang and L. Xie, Chromium Carbide Coatings Produced on Ductile Cast Iron QT600-3 by Thermal Reactive Diffusion in Fluoride Salt Bath: Growth Behavior, Microstructure Evolution and Kinetics, *Ceram. Int.*, 2019, **45**(1), p 1196–1201. https://doi.org/10.1016/J.CERAMINT.2018.09.304

2. J.P. Quintana, J.M. Massone, A.B. Márquez and D.A. Colombo, Rolling Contact Fatigue Behavior of TiN Based Coatings Deposited on ADI by Cathodic Arc Deposition and Plasma Based ion Implantation and Deposition, *Thin Solid Films*, 2019, **671**, p 95–102. https://doi.org/10.1016/J.TSF.2018.12.014

3. F.E. Mariani, C. Soares, A.L. Neto, G.E. Totten and L.C. Casteletti, Boro-Austempering Treatment of Ductile Cast Irons, *Mater. Res.*, 2018 https://doi.org/10.1590/1980-5373-MR-2017-0927

4. D.A. Colombo, R.C. Dommarco and A.D. Basso, Rolling Contact Fatigue Behavior of Dual-Phase Austempered Ductile Iron, *Wear*,

2019, **418–419**, p 208–214. https://doi.org/10.1016/J.WEAR.2018.11.009

5. B. Wang, G.C. Barber, F. Qiu, Q. Zou and H. Yang, A Review: Phase Transformation and Wear Mechanisms of Single-Step and Dual-Step Austempered Ductile Irons, *J. Mater. Res. Technol.*, 2020, **9**(1), p 1054–1069. https://doi.org/10.1016/J.JMRT.2019.10.074

6. G. Angella, D. Ripamonti and M. Górny, Comparison Between Ductility Examination and a New Approach Based on Strain Hardening Analysis to Support the Determination of Proper Austempering Times, *Int. J. Cast Met. Res.*, 2020, **33**(1), p 50–60. https://doi.org/10.1080/13640461.2020.1746041

7. A. Günen, B. Kurt, P. Milner and M.S. Gök, Properties and Tribological Performance of Ceramic-Base Chromium and Vanadium Carbide Composite Coatings, *Int. J. Refract. Met. Hard Mater.*, 2019, **81**, p 333–344. https://doi.org/10.1016/J.IJRMHM.2019.03.019

8. P.A. Dearnley, A. Matthews and A. Leyland, *Tribological Behaviour of Thermochemically Surface Engineered Steels*, Elsevier Inc., Amsterdam, 2015

9. C.K.N. Oliveira, R.M. Muñoz Riofano and L.C. Casteletti, Micro-Abrasive Wear Test of Niobium Carbide Layers Produced on AISI H13 and M2 Steels, *Surf. Coatings Technol.*, 2006, **200**(16–17), p 5140–5144. https://doi.org/10.1016/J.SURFCOAT.2005.05.037

10. Z.J. Shan, Z.G. Pang, F.Q. Luo and F.D. Wei, Kinetics of V(N, C) and Nb(N, C) Coatings Produced by V-Nb–RE Deposition Technique, *Surf. Coatings Technol.*, 2012, **206**(19–20), p 4322–4327. https://doi.org/10.1016/J.SURFCOAT.2012.04.057

11. F.A.P. Fernandes, J. Gallego, C.A. Picon, G. Tremiliosic Filho and L.C. Casteletti, Wear and Corrosion of Niobium Carbide Coated AISI 52100 Bearing Steel, *Surf. Coatings Technol.*, 2015, **279**, p 112–117. https://doi.org/10.1016/J.SURFCOAT.2015.08.036

12. X.S. Fan, Z.G. Yang, Z.X. Xia, C. Zhang and H.Q. Che, The Microstructure Evolution of VC Coatings on AISI H13 and 9Cr18 Steel by Thermo-Reactive Deposition Process, *J. Alloys Compd.*, 2010, **505**(1), p L15–L18. https://doi.org/10.1016/J.JALLCOM.2010.06.064

13. B. Lenz, H. Hasselbruch and A. Mehner, Automated Evaluation of Rockwell Adhesion Tests for PVD Coatings Using Convolutional Neural Networks, *Surf. Coatings Technol.*, 2020, **385**, p 125365. https://doi.org/10.1016/J.SURFCOAT.2020.125365

14. K. Zheng et al., Design and Fabrication of HfC, SiC/HfC and HfC-SiC/HfC Interlayers for Improving the Adhesion Between Diamond Coatings and Cemented Carbides, *J. Alloys Compd.*, 2020, **815**, p 152405. https://doi.org/10.1016/J.JALLCOM.2019.152405

15. F.E. Mariani, R.T. Aureliano, L.C. Casteletti, A.N. Lombardi and G.E. Totten, Characterization and Wear Performance of Borided AISI 304 and UNS S31254 Stainless Steels, *Mater. Perform. Charact.*, 2017 https://doi.org/10.1520/MPC20160096

16. T. Arai, H. Fujita, Y. Sugimoto and Y. Ohta, Diffusion Carbide Coatings Formed in Molten Borax Systems, *J. Mater. Eng.*, 1987, **9**(2), p 183–189. https://doi.org/10.1007/BF02833709

17. X.S. Fan, Z.G. Yang, C. Zhang, Y.D. Zhang and H.Q. Che, Evaluation of Vanadium Carbide Coatings on AISI H13 Obtained by Thermo-Reactive Deposition/Diffusion Technique, *Surf. Coatings Technol.*, 2010, **205**(2), p 641–646. https://doi.org/10.1016/J.SURFCOAT.2010.07.065

18. C.K.N. Oliveira, C.L. Benassi and L.C. Casteletti, Evaluation of Hard Coatings Obtained on AISI D2 Steel by Thermo-Reactive Deposition Treatment, *Surf. Coatings Technol.*, 2006, **201**(3–4), p 1880–1885. https://doi.org/10.1016/J.SURFCOAT.2006.03.036

19. A. OrjuelaG, R. Rincón and J.J. Olaya, Corrosion Resistance of Niobium Carbide Coatings Produced on AISI 1045 Steel via Thermo-Reactive Diffusion Deposition, *Surf. Coatings Technol.*, 2014, **259**(PC), p 667–675. https://doi.org/10.1016/J.SURFCOAT.2014.10.012

20. M. Shirinbayan, A. Shafyei and M.R. Aboutalebi, Kinetics of Vanadium Carbide Coating Produced on AISI D2 Steel by Thermore-active Diffusion Technique, *Russ. J. Appl. Chem.*, 2015, **87**(12), p 1930–1935. https://doi.org/10.1134/S1070427214120222

21. Z. Tao Huang and W. Huai Tian, Effects of Mo Contents in Matrix on Microstructure and Properties of Vanadium Carbide Coating Formed by Thermal Diffusion Treatment, *J. Iron Steel Res. Int.*, 2014, **21**(1), p 104–108. https://doi.org/10.1016/S1006-706X(14)60016-9

22. S.J. Lee, D.K. Matlock and C.J. Van Tyne, An Empirical Model for Carbon Diffusion in Austenite Incorporating Alloying Element Effects, *ISIJ Int.*, 2011, **51**(11), p 1903–1911. https://doi.org/10.2355/ISIJINTERNATIONAL.51.1903

23. W.L. Worrell and J. Chipman, The Free Energies of Formation of the Vanadium, Niobium, and Tantalum Carbides, *J. Phys. Chem.*, 1964, **68**(4), p 860–866. https://doi.org/10.1021/J100786A027

24. C.K.N. Oliveira, R.M.M. Riofano and L.C. Casteletti, Formation of Carbide Layers on AISI H13 and D2 Steels by Treatment in Molten Borax Containing Dissolved both Fe–Nb and Fe–Ti Powders, *Mater. Lett.*, 2005, **59**(14–15), p 1719–1722. https://doi.org/10.1016/J.MATLET.2005.01.052

25. R. Soltani, M.H. Sohi, M. Ansari, A. Haghighi, H.M. Ghasemi and F. Haftlang, Evaluation of Niobium Carbide Coatings Produced on AISI L2 Steel Via Thermo-Reactive Diffusion Technique, *Vacuum*, 2017, **146**, p 44–51. https://doi.org/10.1016/J.VACUUM.2017.09.023

26. M.B. Yang, L.W. Tang, H. Yang and W.L. Zhao, Microstructure and Properties of Surface Coating for Cr12MoV Steel Treated by TD Salt-Bath Vanadizing Process, *Key Eng. Mater.*, 2008, **373–374**, p 196–199. https://doi.org/10.4028/WWW.SCIENTIFIC.NET/KEM.373-374.196

27. C. Soriano, J. Leunda, J. Lambarri, V. GarcíaNavas and C. Sanz, Effect of Laser Surface Hardening on the Microstructure, Hardness and Residual Stresses of Austempered Ductile Iron Grades, *Appl. Surf. Sci.*, 2011, **257**(16), p 7101–7106. https://doi.org/10.1016/J.APSUSC.2011.03.059

28. F.V. Guerra, L.A. Bedolla-Jacuinde, I. Mejía, J. Zuno and C. Maldonado, Effects of Boron Addition and Austempering Time on Microstructure, Hardness and Tensile Properties of Ductile Irons, *Mater. Sci. Eng. A*, 2015, **648**, p 193–201. https://doi.org/10.1016/J.MSEA.2015.09.066

29. K. Nakamura and M. Yashima, Crystal Structure of NaCl-Type Transition Metal Monocarbides MC (M = V, Ti, Nb, Ta, Hf, Zr), a Neutron Powder Diffraction Study, *Mater. Sci. Eng. B*, 2008, **148**(1–3), p 69–72. https://doi.org/10.1016/J.MSEB.2007.09.040

30. J.F. Archard, Contact and Rubbing of Flat Surfaces, *J. Appl. Phys.*, 2004, **24**(8), p 981. https://doi.org/10.1063/1.1721448